

Deep Meridional Overturning Circulation in the Indian Ocean and Its Relation to Indian Ocean Dipole

WEIQIANG WANG

State Key Laboratory of Tropical Oceanography, South China Sea Institute of Oceanology, Chinese Academy of Sciences, Guangzhou, China

XIUHUA ZHU

Center für Erdsystemforschung und Nachhaltigkeit, KlimaCampus, University of Hamburg, Hamburg, Germany

CHUNZAI WANG

NOAA/Atlantic Oceanographic and Meteorological Laboratory, Miami, Florida

ARMIN KÖHL

Institut für Meereskunde, Center für Erdsystemforschung und Nachhaltigkeit, KlimaCampus, University of Hamburg, Hamburg, Germany

(Manuscript received 7 August 2013, in final form 12 March 2014)

ABSTRACT

This paper uses the 42-yr German Estimating the Circulation and Climate of the Ocean (GECCO) synthesis data to analyze and examine the relationship of the Indian Ocean deep meridional overturning circulation (DMOC) with the Indian Ocean dipole mode (IOD). Contributions of various dynamical processes are assessed by decomposing the DMOC into the Ekman and geostrophic transport, the external mode, and a residual term. The first three terms successfully describe the DMOC with a marginal residual term. The following conclusions are obtained. First, the seasonal cycle of the DMOC is mainly determined by the Ekman component. The exception is during the transitional seasons (March–April and September–October) in the northern Indian Ocean Basin, where the geostrophic component dominates. Second, at the beginning phase of the IOD (May–June), the Ekman component dominates the DMOC structure; at and after the peak phase of the IOD (September–December), the DMOC structure is primarily determined by the geostrophic component in correspondence with the well-developed sea surface temperature anomalies, while the wind (and thus the Ekman component) plays a secondary role south of 10°S and contributes negatively within the zonal band of 10° on both sides of the equator. Therefore, there exists a surface to deep-ocean connection through which IOD-related surface wind and ocean temperature anomalies are transferred down to the deep ocean. Westward-propagating signals are observed even in the deep ocean, suggesting possible roles of Rossby waves in transferring the surface signal to the deep ocean.

1. Introduction

A deep meridional inflow is one of the characteristic features at the southern Indian Ocean where North Atlantic Deep Water, Antarctic Bottom Water, and Circumpolar Deep Water enter the Indian Ocean in the

western basin off Madagascar and off the coast of East Africa and in the east along the Ninety East Ridge (Mantyla and Reid 1995; Schott and McCreary 2001). Because of sparse observations in the deep Indian Ocean, the Indian Ocean deep meridional overturning circulation (DMOC) and its temporal and spatial variability remain open to be investigated in a more systematic manner.

The time-mean structure of the DMOC was earlier obtained based on individual transoceanic hydrographic sections, either by estimating the geostrophic transports

Corresponding author address: Xiuhua Zhu, KlimaCampus, Hamburg University, Grindelberg 5, D-20144 Hamburg, Germany.
E-mail: xiuhua.zhu@zmaw.de

(Toole and Warren 1993; Robbins and Toole 1997) or via an inverse box modeling approach (Macdonald 1998; Ganachaud et al. 2000; Bryden and Beal 2001; Sloyan and Rintoul 2001; Ganachaud 2003; Lumpkin and Speer 2007; McDonagh et al. 2008). Since both approaches depend heavily on hydrographic data sections, which are often sparse in the spatial and temporal resolution, their results are often contaminated by strong seasonal variability in the Indian Ocean. In comparison, numerical model efforts as an alternative way show weak but noticeable time-mean bottom inflow [2–5 Sv (1 Sv $\equiv 10^6 \text{ m}^3 \text{ s}^{-1}$); Garternicht and Schott 1997; Lee and Marotzke 1998; Stammer et al. 2002; Drijfhout and Garabato 2008; Wang et al. 2012]. One exception is the estimation of 17 Sv from Ferron and Marotzke (2003), which has been shown to be not maintainable when the initial conditions and forcing fields modified by an adjoint method are applied for several hundred years (Palmer et al. 2007) instead of for a few years, as in Ferron and Marotzke (2003). On the other hand, it has also been acknowledged that, although numerical model results are dynamically consistent, they are conditioned to prescribed weak vertical mixing, different surface heat and momentum fluxes products, model resolution, open boundary conditions, and deficits with respect to the bottom water formation (Schott and McCreary 2001; Drijfhout and Garabato 2008; Rintoul et al. 2010; Wang et al. 2010).

The DMOC displays large seasonal variations over most latitudes and is characterized by two counter-rotating meridional overturning cells (Lee and Marotzke 1998; Wang et al. 2012): In boreal winter, one cell is anti-clockwise (facing the paper, unless otherwise specified), residing in the region south of 20°S, and the other is clockwise, residing in the interior Indian Ocean centered on 10°S. Both cells reverse their rotation in boreal summer in response to the seasonal monsoon reversal. The overturning streamfunction almost covers the whole water column year-round, indicating the deep-reaching effect of the Indian monsoon (Schott et al. 2002).

The Indian Ocean DMOC also exhibits pronounced interannual variability. Significant 2-yr variation has been found in the DMOC (Wang et al. 2012) as well as in other essential oceanic variables, such as sea surface temperature (SST) (Feng and Meyers 2003) and meridional ocean heat transport in the equatorial Indian Ocean (Chirokova and Webster 2006), which is reminiscent of the tropospheric biennial oscillation (TBO; Meehl and Arblaster 2002; Loschnigg et al. 2003). The DMOC highly correlates with the most prominent interannual mode, the Indian Ocean dipole mode (IOD) (Wang et al. 2012), whose positive phase is characterized by negative SST anomalies in the tropical southeastern

Indian Ocean and positive SST anomalies in the tropical western Indian Ocean.

The characteristic dipole SST pattern of IOD events occurs first in May–June and peaks in September–October; its demise is likely due to the monsoonal reversal that weakens winds both along the equator and along the Indonesian coast, diminishing the importance of ocean dynamics in the regulation of SST (Saji et al. 1999). Acknowledging that the IOD is parented by an anomalous monsoon through the generation of zonal temperature gradients between upwelling regions, Webster et al. (1999, 2002) suggest that the east–west SST gradients initiated by the anomalous monsoon intensity can lead to the enhancements of the zonal SST gradients by modulating local upwelling and meridional oceanic heat transport through involving equatorial wave dynamics. In this respect, they suggest the IOD to be an integral part of the TBO, because it could regulate the intensity of the monsoon system, introduce slow dynamics into the monsoon-initiated SST anomalies, and help to penetrate these anomalies to the next year.

In this study, by decomposing the DMOC into three dynamical components and assessing their relative contributions, we show that the Indian Ocean DMOC is dynamically linked to ocean surface conditions mainly through wind (thus the Ekman component) on seasonal scales and through both wind and sea temperature anomalies on (IOD related) interannual time scales. We extend the traditional view of the air–sea coupled system in the Indian Ocean, which is merely confined to the upper Indian Ocean and the overlying atmosphere so far (Webster et al. 2002; Feng and Meyers 2003; Loschnigg et al. 2003; Annamalai and Murtugudde 2004; Pillai 2008), to the deep ocean. This paper is organized as follows: section 2 describes data and methodology; section 3 presents results about the roles of various dynamical components of the DMOC during IOD events; section 4 gives a discussion; and section 5 provides a summary and conclusions.

2. Data and methodology

a. Data

The ocean dataset used in this study is based on products from the German Estimating the Circulation and Climate of the Ocean (GECCO) consortium efforts (Stammer et al. 2004; Köhl et al. 2006, 2007). The estimate is available for a quasi-global ($\pm 80^\circ$ latitude) domain with 1° spatial resolution and spans the period 1952–2001. It is obtained by combining most of the global observations available during the entire estimation period with the ECCO model by changing the initial temperature and salinity fields over the full water

column and by adjusting the National Centers for Environmental Prediction (NCEP) time-varying surface forcing over the full estimation period so as to simulate best the observed ocean state. Details of the GECCO optimization are described by Köhl and Stammer (2008a,b). The time scales of associated adjustment processes are typically 5–7 yr; therefore, we discard the first 8 yr and analyze the data from 1960 to 2001.

b. DMOC index

To identify water mass property in different ocean layers, the neutral densities of $\gamma^t = 27.05$, 27.72, and 28.11 kg m^{-3} are chosen to separate the water column into the upper ($\gamma^t < 27.05$), intermediate ($27.05 \leq \gamma^t < 27.72$), deep ($27.72 \leq \gamma^t < 28.11$), and bottom layers ($\gamma^t \geq 28.11$) (Ganachaud and Wunsch 2000; Ganachaud et al. 2000). The upper surface of the bottom water ($\gamma^t = 28.11$) is generally deeper than 3100 m (Wang et al. 2012). The deepest depth is below 3350 m in the Somali Basin and the Arabian Basin, around 3100–3200 m in the Crozet Basin and the Madagascar Basin, and around 3150–3300 m in the central Indian Ocean Basin and the West Australian Basin (Wang et al. 2012). In later sections, the total volume transport of the bottom layer ($\gamma^t \geq 28.11$) across 34°S is used to measure the strength of the DMOC. It has a mean of around 2.1 Sv (Wang et al. 2012). Note that the existence of the Indonesian Throughflow (ITF) does not affect the strength of the DMOC index, because it occurs at densities lighter than $\gamma^t = 28.0 \text{ kg m}^{-3}$.

c. DMOC decomposition

Following Lee and Marotzke (1998) and Hirschi and Marotzke (2007), the Indian Ocean DMOC is decomposed into geostrophic, Ekman, and external components, assuming that the residual term accounting for ageostrophic contributions (in addition to the Ekman component) is negligible. The method has been used previously to study the seasonal cycle of meridional overturning and heat transport of the Indian Ocean (Lee and Marotzke 1998). In this study, we apply it to the climatological fields on a bimonthly basis and subsequently calculate composites of all three terms for IOD events to assess their relative contributions.

The DMOC is decomposed into four components in Eq. (1) [essentially Eq. (16) in Hirschi and Marotzke 2007]: (i) Ekman component φ_{ek} , (ii) geostrophic component φ_{geo} , (iii) external mode φ_{ex} , and (iv) residual term φ_{res} :

$$\varphi = \varphi_{\text{ek}} + \varphi_{\text{geo}} + \varphi_{\text{ex}} + \varphi_{\text{res}}, \quad (1)$$

$$\varphi_{\text{ek}} = \int_{-H}^{z'} dz \int_{x_w}^{x_e} (v_{\text{ek}} - \bar{v}_{\text{ek}}) dx, \quad (2)$$

$$\bar{v}_{\text{ek}} = -\frac{1}{\rho^* f A} \int_{x_w}^{x_e} \tau^x dx, \quad (3)$$

$$\varphi_{\text{geo}} = \int_{x_w}^{x_e} dx \int_{-H}^{z'} (\tilde{v} - \bar{v}_g) dz, \quad (4)$$

$$\tilde{v}(x, z') = -\frac{g}{\rho^* f} \int_{-H}^{z'} \frac{1}{L(z)} (\rho_e - \rho_w) dz, \quad (5)$$

$$\bar{v}_g(x) = \frac{1}{H(x)} \int_{-H(x)}^0 \tilde{v}(z, x) dz, \quad (6)$$

$$\varphi_{\text{ex}} = \int_{-H}^{z'} dz \int_{x_w}^{x_e} \bar{v} dx, \quad \text{and} \quad (7)$$

$$\bar{v} = \frac{1}{H} \int_{-H}^0 v dz, \quad (8)$$

where x_w and x_e are the western and eastern boundaries of the Indian Ocean Basin, respectively, and $-H \ll z' \leq 0$; A is the total area of the corresponding longitude–depth section of the ocean basin; and ρ^* , f , L , and τ^x are a reference density, the Coriolis parameter, the basin width at the surface, and the zonal wind stress, respectively. The residual term φ_{res} in Eq. (1) is calculated as a residue of the other three terms.

The Ekman velocity v_{ek} is compensated by a barotropic return flow \bar{v}_{ek} [Eqs. (2) and (3)]; the geostrophic velocity \tilde{v} describes the thermal wind shear balanced by zonal density gradients [Eqs. (4)–(6)], and its depth average \bar{v}_g is removed in Eq. (6). Note that this term should be zero if the assumption of zero bottom velocity is met. The external mode φ_{ex} describes the depth-averaged meridional flow [Eqs. (7) and (8)] and contributes to the DMOC in the presence of topography (Hirschi and Marotzke 2007); φ_{res} contains small ageostrophic terms and errors resulting from imperfect sampling.

Note that only the external component may integrate over the section to a nonzero volume transport because of the freshwater exchange with the atmosphere and the cross-basin exchange through the ITF. The former amounts to zero since only salt flux is used in GECCO, whereas the latter contributes to both the external and geostrophic components. In the GECCO dataset, the ITF enters the Indian Ocean between 9° and 20°S, has a climatological mean of 9.2 Sv and a standard deviation of 3.6 Sv (Wang et al. 2012). Since most of the ITF transport is present in the upper around 400 m (Liu et al. 2005), we integrate the mass streamfunction from the ocean bottom upward such that ITF's influence is confined within the upper ocean. However, this confinement through the upward integration pertains only to ITF's contribution to the geostrophic component. Its

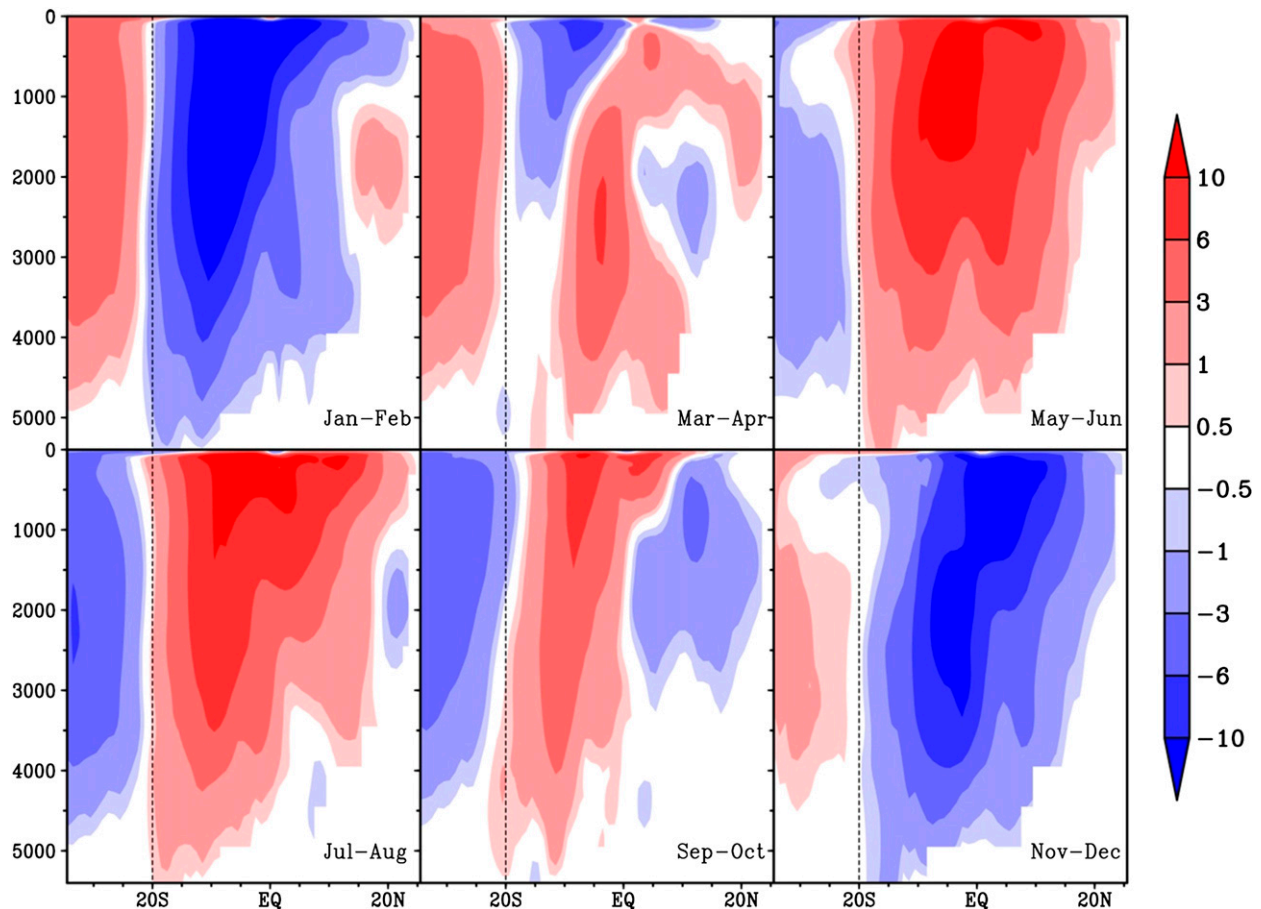


FIG. 1. Bimonthly-mean meridional overturning transport streamfunctions of the Indian Ocean DMOC (Sv). The y axis denotes ocean depth in meters. The meridional overturning streamfunction corresponds to the mass flux integrated from the bottom to surface and then zonally integrated in the Indian Ocean.

contribution to the external component [Eq. (7)] enters through its projection onto the zonally nonuniform depth-averaged meridional velocity [Eq. (8)], because a big portion of the ITF joining the South Equatorial Current reaches the western part of the Indian Ocean Basin and mainly flows southward (from both sides of Madagascar). Given the zonally varying topography, the resultant zonally nonuniform meridional velocity constitutes part of the external mode [Eq. (8)]. This may be better envisioned with the aid of two examples provided by Lee and Marotzke (1998): 1) When a western boundary current travels northward along a coast having a depth of 1000 m and the return flows go southward over much greater depths, the zonal integration will result in an overturning characterized by a net northward flow above 1000 m and southward flow below it. 2) The zonal component of a horizontal barotropic gyre going over zonally nonuniform topography will cause net upwelling or downwelling upon zonal integration.

3. DMOC variations during IOD events

To focus on interannual variations, a high-pass Butterworth filter with a cutoff frequency of 7 yr is applied to the meridional streamfunction, SST, and the wind stress field at each model grid for the 1960–2001 period. Components longer than 7 yr of these variables, which have been removed through the high-pass filtering, are presented in Fig. 3, while the rest of the analysis (except Fig. 8) refers to the high-pass filtered variables. As a result, two dominant interannual periodicities, in addition to seasonal cycles, are retained in our analysis: 2–3 yr corresponding to TBO and 3–7 yr corresponding to ENSO (Pillai and Mohankumar 2009). Note that prior to the composite analysis, the high-pass filtered variables are further subject to deseasonalization; that is, the monthly climatological states shown in Figs. 1 and 2 are removed from the respective variable.

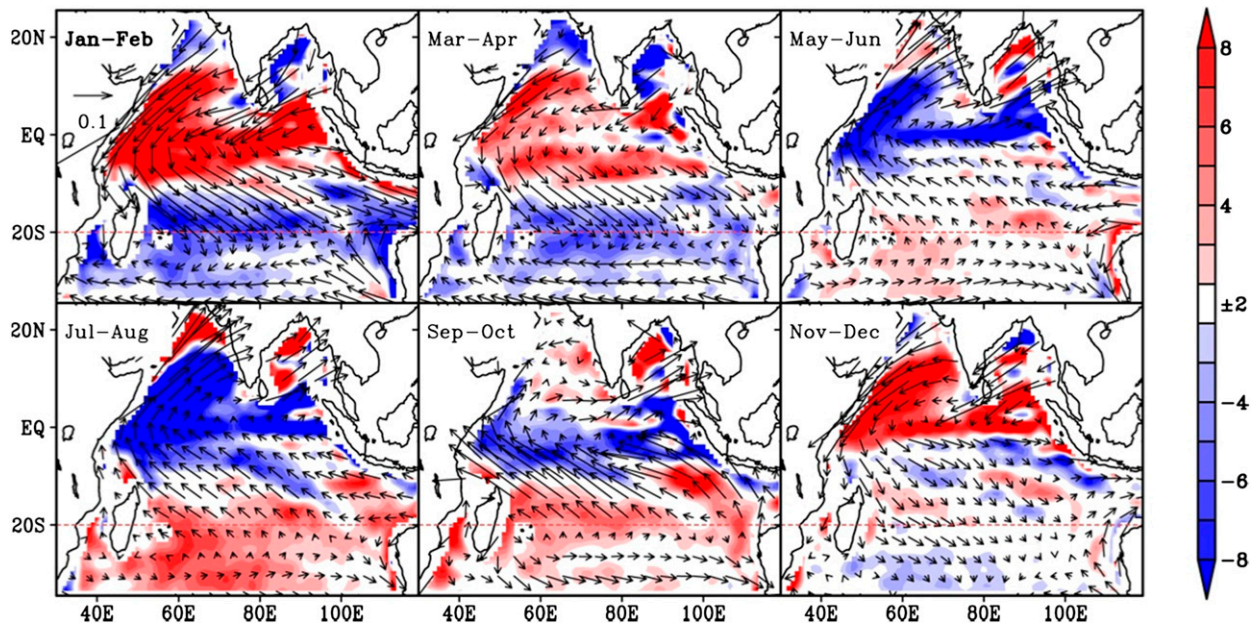


FIG. 2. Bimonthly-mean wind stress (vector; N m^{-2}) and wind stress curl (shaded; $1 \times 10^{-8} \text{ N m}^{-3}$) in the Indian Ocean.

a. Climatological states: DMOC and surface wind

We first present the annual cycle of the high-pass filtered Indian Ocean deep meridional streamfunctions (Fig. 1). Double counterrotating meridional overturning cells are most obvious in boreal winter (from November to February) and summer (from May to August), while in transitional seasons (March–April and September–October) the northern cell splits into two parts. In boreal winter, a clockwise closed deep cell dominates the interior ocean (north of 20°S) and an anticlockwise deep cell locates in the southern Indian Ocean (south of 20°S), both of which reverse their rotations in boreal summer in response to the reversal to the summer monsoon. This pair of deep cells covers the entire water column with maximum strength of $10\text{--}12 \text{ Sv}$ at 1000-m depth (located between 10°S and 5°N) and is noticeably separated at around 20°S year-round.

Figure 2 shows bimonthly means of wind stress and wind stress curl. In boreal winter (from November to February), positive wind stress curl occurs north of 10°S and negative wind stress curl occurs to its south with maximum centered along 20°S . The wind stress curl pattern in boreal summer resembles that in winter months but with opposite signs. According to Ekman dynamics, positive (negative) maximum curl corresponds to maximum downwelling (upwelling) in the Southern Hemisphere, as has been manifested by confluences of upward (downward) branches of both cells near 20°S (Fig. 1).

Note that the climatological features shown in Figs. 1 and 2 are derived from the high-pass filtered variables

with a cutoff frequency of 7 yr. The low-frequency wind component ($\geq 7 \text{ yr}$), primarily characterized by southeasterlies in the southern Indian Ocean (Fig. 3b) and strong westerlies over the circumpolar ocean (not shown), persists throughout the year and may relate to the southern annular mode (Thompson and Wallace 2000). The resultant Ekman drift leads to convergence and downwelling between 60° and 20°S (where the maximum easterly component sits) and divergence and upwelling between the equator and 20°S , which accounts for an upwelling (positive) cell within the southern Indian Ocean domain with maximum amplitude of around 2 Sv in the deep ocean (Fig. 3a).

b. Climatological states: DMOC and its dynamical components

The climatological Indian Ocean DMOC structure is to a great extent captured by reconstructions from the first three terms on the right side of Eq. (1) with a reasonably small residual term (Figs. 1 and 4d). Ekman components determine the main structure of the DMOC and account for a large part of the amplitude throughout all months (Fig. 4a). Exceptions are in transitional seasons (March–April and September–October) in the northern Indian Ocean Basin, where the geostrophic component offsets the Ekman contribution and dominates the local DMOC structure (Fig. 4b).

The external component shows two main features. First, a coherent pattern lies south of 20°S throughout the year, extending to 5000 m , and is in phase with

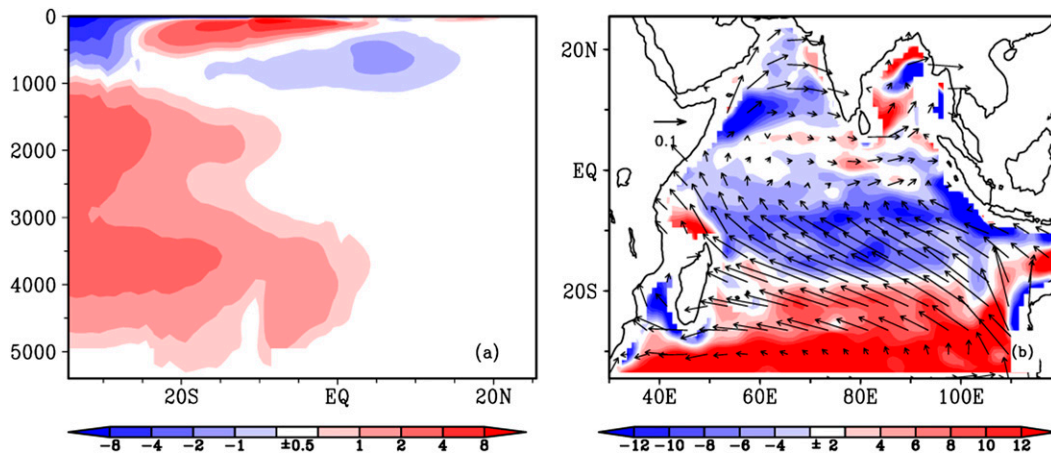


FIG. 3. As in (left) Fig. 1 and (right) Fig. 2, but for components larger than 7 yr, which remain almost unchanged through the annual course. The y axis in (a) denotes ocean depth in meters.

Ekman contributions most of the year. Second, its spatial features in summer (May–October) and winter (November–April) months are rather similar but with opposite signs. Both features reflect only, because of zonal topographic gradients, changes in horizontal ocean gyre, or in cross-basin zonal gradients of the depth-independent meridional velocity in relation to the summer/winter monsoon shift.

In summary, the seasonal DMOC structure can be satisfactorily reconstructed from its three dynamical components: the Ekman flow and its barotropic compensation, the thermal wind component, and the depth-independent external mode. In the following, relative contributions of these three dynamical components to the DMOC are assessed each month and subject to a composite analysis to obtain a quantitative estimate of their roles in relation to IOD events.

c. Positive IOD composites

Possible imprints of IOD events on the Indian Ocean DMOC are studied by means of the composite analysis for strong positive IOD events. These selected events are first subject to deseasonalization: that is, climatological monthly DMOC as shown in Fig. 1 is removed prior to the composite analysis.

The IOD strength is measured by zonal sea surface temperature (SST) differences between the tropical western Indian Ocean (50° – 70° E, 10° S– 10° N) and the tropical southeastern Indian Ocean (90° – 110° E, 10° S– 0°), following the same definition as in Saji et al. (1999). Figure 5 shows the time series of the IOD index along with that of the Indian Ocean DMOC index that is represented by the volume transport of the bottom flow ($\gamma^n \geq 28.11 \text{ kg m}^{-3}$) across 34° S. Both time series are smoothed by a 7-month running average. With the

threshold of 1.5 (multiplied by the standard deviation), we obtain nine positive IOD (1965, 1967, 1972, 1976, 1977, 1982, 1987, 1994, and 1997). In most cases, the DMOC index is out of phase with the IOD index, whereas the years 1965 and 1987 are exceptional. To highlight the commonality of majority cases, we exclude the years 1965 and 1987, thus keeping seven positive IOD cases in the following composite calculations.

Figure 6 shows the characteristic evolution of the dipole SST anomaly pattern, consistent with IOD features described by Saji et al. (1999). Cold SST anomalies first occur in May off the Java coast, accompanying stronger-than-normal alongshore southeasterlies and easterly anomalies along the equator between 80° and 100° E. Previous studies have revealed twofold effects of these wind anomalies: the stronger-than-normal alongshore southeasterly wind leads to stronger coastal upwelling off Java and Sumatra while the easterly anomalies along the equator hamper the eastward intrusion of the equatorial current, thus reducing heat supply to the east. Both effects further enhance cooling off Indonesia, where the shoaling thermocline provides another prerequisite for this cooling (Xie et al. 2002). This process may relate to both ocean advection and equatorial and coastal Kelvin wave dynamics (e.g., Feng and Meyers 2003). For example, Xie et al. (2002) reported that a westward downwelling Rossby wave forced by the IOD-associated wind stress curl leads to deepened thermocline and thus warmer SST in the west, which is further intensified on the surface because of reduced wind speed and evaporation induced by anomalously northwestward-extended southeasterly trade winds (Saji et al. 1999). Therefore, changes of the southeast trade winds on the equatorial region coupled with SST anomalies through ocean dynamics give rise to SST

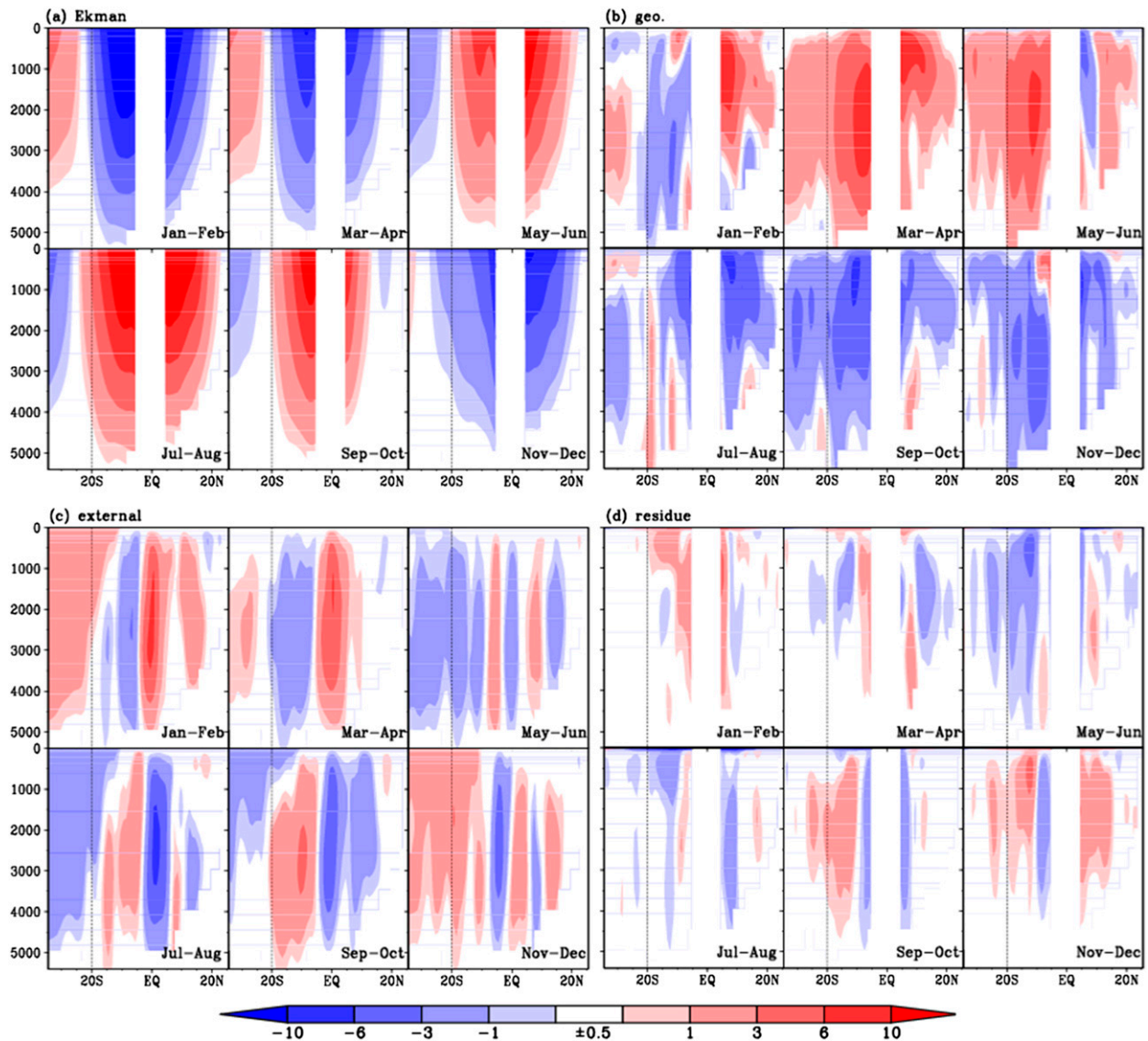


FIG. 4. Bimonthly decompositions of the DMOC into contributions from (a) the Ekman component, (b) the geostrophic component, (c) the external mode, and (d) the residual term. The y axis denotes ocean depth in meters.

dipole events. The major role of equatorial wave dynamics in regulating the dipole SST pattern is partly manifested by the westward propagation of cold SST anomalies along 10°S from September to December (Fig. 6). On the other hand, the IOD-related atmospheric circulation essentially reflects the zonal pressure difference in the equatorial Indian Ocean; thus, it is closely related to changes in equatorial wind systems, such as the Walker circulation (Saji and Yamagata 2003).

In September–October northwesterly wind anomalies appear in the central southern Indian Ocean indicating weakening of the prevailing southeasterly trade winds (Fig. 6). Together with the easterly wind anomalies along the equator, they form an anticlockwise wind

stress curl generating anomalous Ekman pumping within the zonal band from the equator to 20°S . This positive wind stress curl extends farther westward along the equator in November–December and occupies almost the entire southern tropical Indian Ocean (Fig. 6).

In May–June, the DMOC composite is characterized by a dipole demarcated at around 10°S ; the related anomalies almost vanish in July–August and show no distinguishable spatial patterns (Fig. 7a). In September–October, an anomalous negative cell occurs between 20°S and the equator, which expands in November–December into the entire southern Indian Ocean Basin accompanied by a positive cell in the upper 2000 m in the northern Indian Ocean (Fig. 7a).

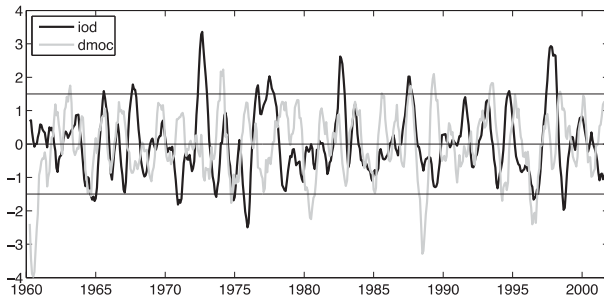


FIG. 5. Time series of the IOD (black) and the DMOC index (gray) during 1960–2001. Variability longer than 7 yr is removed and the 7-month running mean is applied. Both time series are normalized and therefore unitless. Three horizontal lines mark 1.5, 0, and -1.5 , respectively.

The IOD-related DMOC features shown above are, to a large extent, described by the reconstruction following Eq. (1) (Figs. 7a,e,f). Each dynamical component of the DMOC plays varying roles at different IOD phases. For example, in May–June, the DMOC anomalies are mainly contributed by Ekman components characterized by a pair of two reversely rotating cells separated at 10°S (Fig. 7b), but in later months it is geostrophic current that determines the spatial feature of the DMOC anomalies; in particular, the more

stratified DMOC structure in November–December in the Southern Ocean Basin is mainly attributed to the geostrophic component (Fig. 7c).

Within 10° on both sides of the equator Ekman-related DMOC anomalies are offset by thermal wind contribution, whereas, south of 10°S , Ekman and thermal wind components share the same sign; thus, both contribute positively to the strong negative DMOC anomalies in the southern Indian Ocean (Figs. 7b,c). The external-mode-related DMOC anomaly is primarily confined in the deep southern Indian Ocean (below 1000 m) and has its highest loading near 10°S in September–December (Fig. 7d).

The most pronounced IOD signals are manifested as wind and SST anomalies in the tropical Indian Ocean, as shown in Fig. 6. These two variables link directly to the Ekman and thermal wind components of the DMOC, respectively, through which IOD signals penetrate to the deep ocean. At the starting phase of the IOD events (May–June), the SST anomalies are still weak (Fig. 6) and so are the anomalous thermal wind flows (Fig. 7c). On the other side, the associated anomalous wind stress curl shows cross-basin coherent patterns: zonal bands of positive wind stress curls meet negative wind stress curl anomalies along approximately 10°N and 20°S (Fig. 6),

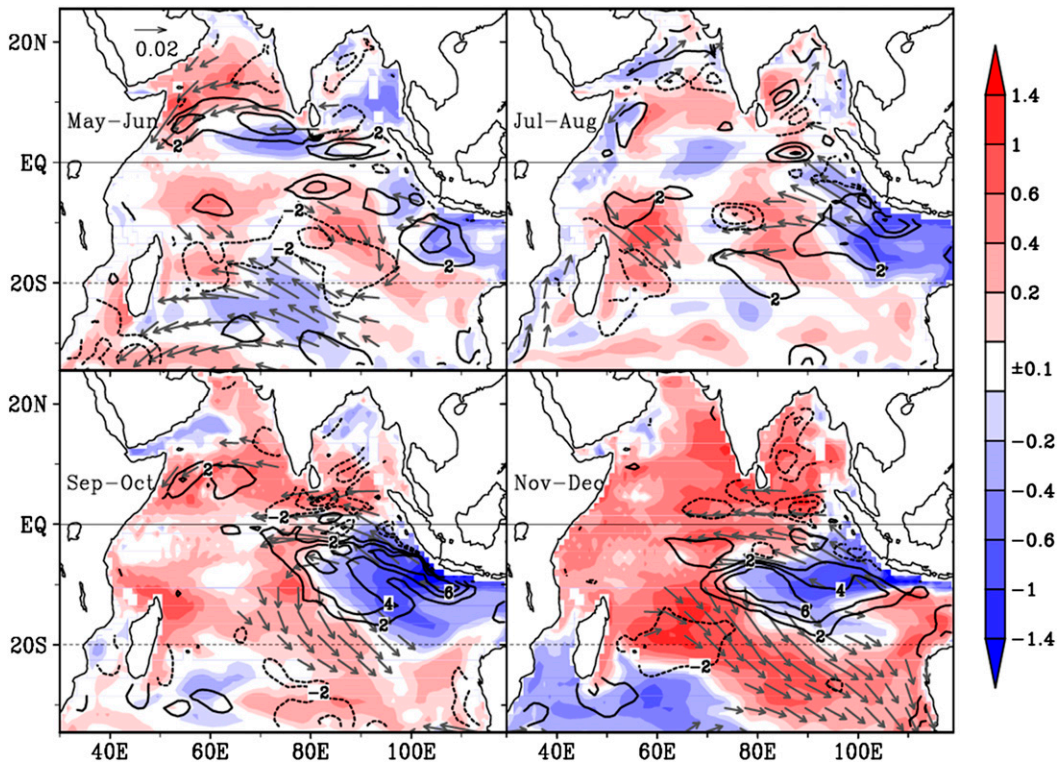


FIG. 6. Positive IOD composites of wind stress anomaly (vectors; only values larger than 0.01 N m^{-2} are shown), SST anomaly (shaded), and wind stress curl anomaly (contour; 10^{-8} N m^{-3}).

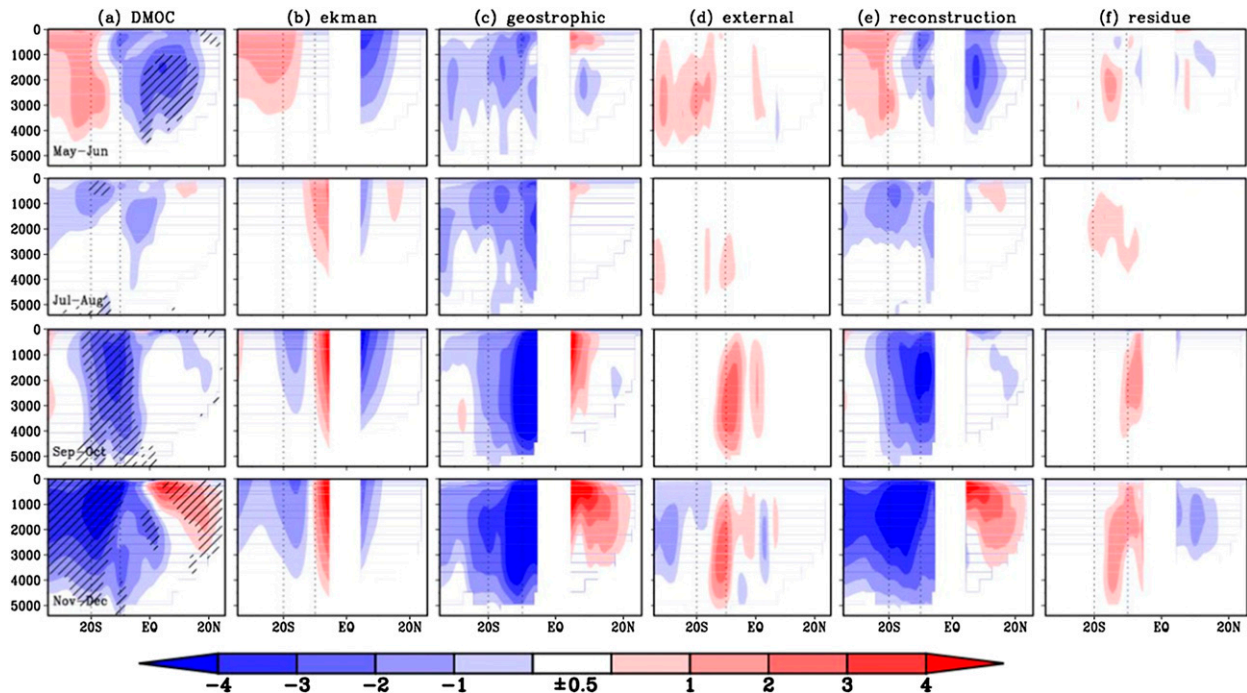


FIG. 7. Positive IOD composites of (a) anomalies of the DMOC strength and contributions from (b) the Ekman component, (c) the geostrophic component, and (d) the external mode. (e) Reconstructions from (b)–(d) and (f) the residual term are also shown. DMOC anomalies exceeding 95% significance (using the Monte Carlo method) are hatched. The significance test is performed as follows: each time 7 years are randomly picked from the 42-yr period (1960–2001), which is repeated for 1000 times. At each grid, the 5% and 95% quartiles from the 1000 series serve as the 95% significance criteria.

resulting in the local DMOC extrema (Fig. 7b). In July–August, the wind stress curl anomaly loses its cross-basin coherent spatial feature (Fig. 6); correspondingly, the Ekman-related DMOC contribution reduces considerably (Fig. 7b). Meanwhile, the cold SST anomaly near the Java coast spreads and enhances further until December (Fig. 6), which is consistent with a strong contribution from the thermal wind component of the DMOC (Fig. 7c).

From September to December, accompanying strengthening and the westward propagation of the cold SST anomalies in the southern tropical Indian Ocean, the anomalous equatorial easterly and northwesterly winds in the southern Indian Ocean strengthen and moreover resume a cross-basin coherent feature with the zero (anomalous) wind stress curl line taking up a northwest–southeast orientation between 10° and 20° S (Fig. 6). This is in correspondence with the negative Ekman component of the DMOC centered along around 15° S (Fig. 7b).

4. Discussion

We have adopted the methodology of Lee and Marotzke (1998) and Hirschi and Marotzke (2007) and

applied it to the Indian Ocean DMOC on both seasonal and the IOD-related time scales. As a supplement to Lee and Marotzke (1998) that discussed the DMOC feature in monsoon-prevailing months (January and July), we also analyzed transitional months when the Asian monsoon reverses its direction (March–April and September–October; Figs. 1–3) and the DMOC features a two-cell structure north of 20° S, in contrast to a coherent structure during monsoon-prevailing months (Fig. 1). In the transitional months, the previous prevailing monsoon weakens and the subsequent monsoon regime is not yet fully established; as a result, the Ekman component weakens, which is more clearly seen north of the equator (Fig. 1), whereas the geostrophic component obtains a coherent structure across the entire Indian Ocean Basin. The latter partly offsets the former and even supersedes it north of 10° S in March–April and north of equator in September–October (Fig. 1), contributing to the two-cell feature north of 20° S in the transitional months.

There is a clear demarcation line around 20° S separating two reversely rotating circulation cells throughout the year (Fig. 1). It reflects the effects of the monsoonal winds and the associated seasonal shift of intertropical convergence zone in the Southern Ocean. This

demarcation line is, however, less pronounced in January and almost indistinguishable in July in Lee and Marotzke 1998 (see their Fig. 10). This difference may stem mainly from the difference in wind products: GECCO datasets used NCEP wind stresses and Lee and Marotzke (1998) used surface fluxes from Hellerman and Rosenstein (1983). It may partly be due to the strong constraints they imposed in the sponge layer in connection to the Antarctic Circumpolar Current (ACC) (Lee and Marotzke 1998). These strong constraints efficiently inhibit not only interannual variability of the ACC but also its interaction with the internal Indian Ocean Basin, which may be nontrivial in shaping the circulation feature in the southern Indian Ocean.

The composite analysis for positive IOD events demonstrates the dynamical link between the Indian Ocean DMOC and ocean surface conditions: namely, the characteristic IOD-related wind and SST anomalies are directly linked to the structure of the DMOC on interannual time scales. By this means, we extend the traditional view of the air–sea coupled system in the Indian Ocean, which is merely confined to the upper Indian Ocean and the overlying atmosphere so far (Webster et al. 2002; Feng and Meyers 2003; Loschnigg et al. 2003; Annamalai and Murtugudde 2004; Pillai 2008), to the deep ocean. Because of such a surface to deep-ocean connection, what occurs on the ocean surface in the form of wind and SST anomalies are dynamically linked to the DMOC variability; therefore, it is not surprising to observe that the DMOC exhibits concentrated energy on time scales that are characteristic of the surface air–sea coupled system, such as on the typical time scales of TBO and ENSO (Wang et al. 2012). The revealed strong contribution of the Ekman component to the Indian Ocean DMOC variability through the year supports the suggestion that large-scale surface wind forcing plays a significant role in sustaining overturning in the deep ocean through mixing processes (Guan and Huang 2008; Huang 1999; Nycander et al. 2007; Huussen et al. 2012).

A question naturally arises: Through which mechanism do IOD-related temperature anomalies influence the deep ocean down to 5000 m, particularly during September through December (as shown in Fig. 7a)? A westward propagation is clearly visible in temperature and meridional velocity fields even at the depth of 3000 m, as is shown in the snapshot of temperature anomalies at 2000 m at 20°S for the period of 1971–73 (Fig. 8). This westward propagation is faster when approaching the equator (not shown). Therefore, we conjecture that the IOD-related surface signal may be carried down in the form of the annual wind-driven Rossby waves, which force the deep ocean by vertical

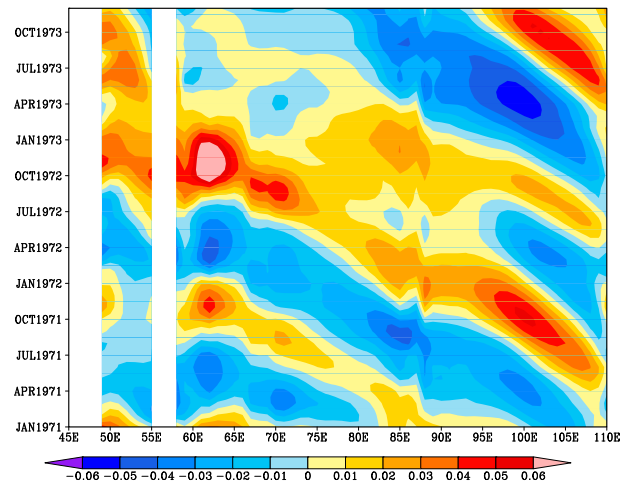


FIG. 8. Hovmöller plot of temperature anomalies at 2000 m at 20°S from 1971 to 1973.

movements of the thermocline because of the wind-driven convergence and divergence in the upper ocean (Kessler and McCreary 1993; Johnson 2011). In fact, a strong presence of annual wind-driven Rossby waves has been observed in hydrographic profiles in the Arabian Sea (Brandt et al. 2002) and in the equatorial Pacific (Kessler and McCreary 1993) and is reported to be coupled with the overlying atmosphere on annual and interannual scales (White 2000a,b, 2001). These annual wind-driven Rossby waves are most likely the messenger responsible for communicating variations on the ocean surface down to the deep ocean. A detailed analysis related to this aspect is planned for future studies.

We would like to stress that the choice of positive IOD events might vary, depending on the dataset and the definition used (e.g., Saji et al. 1999; Saji and Yamagata 2003; Du et al. 2013). The analysis presented here is based on the GECCO ocean reanalysis dataset. Compared to previous studies (e.g., Saji et al. 1999; Saji and Yamagata 2003; Du et al. 2013), we miss the IOD events in 1961 and 1963. We conjecture that the mistargeting in 1961 and 1963 may relate to the slow adjustment to the initial conditions in the assimilation process in the GECCO data. We try to minimize its effect by disregarding the first 8 simulation years (1952–59), which may not be sufficient, as can be seen from the abrupt increase of the DMOC index from 1960 to 1963 (Fig. 5).

Similar analysis has also been performed for negative IOD cases. Based on the threshold of -1.5 , six negative IOD events are selected: 1964, 1970, 1973, 1975, 1996, and 1998 (Fig. 5). A closer look at the annual course of the IOD index shows that positive and negative IOD events are not symmetric around zero (Fig. 9). While all of the selected positive IOD events mature in autumn,

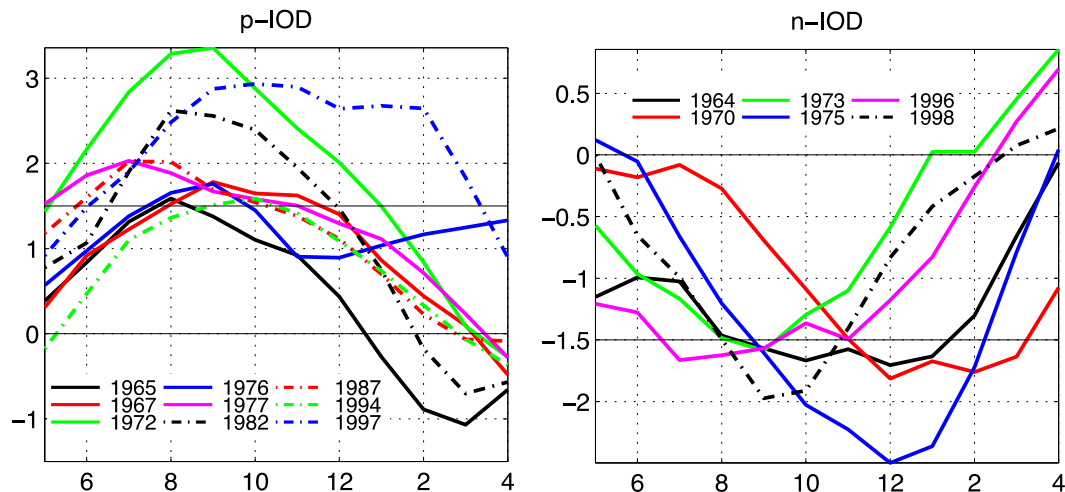


FIG. 9. Evolution course of the IOD index from May to April of the respective following year for (left) positive IOD events (nine cases) and (right) negative IOD events (six cases). Colors represent different years. Horizontal lines mark 0 and 1.5 in (left) and -1.5 and 0 in (right).

three out of six negative IOD events (1964, 1970, and 1975) reach the minimum between December and March of the following year and in 1973 and 1998 the minimum IOD index appears near September. This asymmetry between the opposite phases of the IOD has already been noticed by many studies (e.g., Ummenhofer et al. 2013). Although the DMOC index also shows an out-of-phase relation with the IOD index during most of the negative IOD events (Fig. 5), the wide spread of the development course of negative IOD events makes the interpretation of the time-based composite less meaningful. Therefore, the results presented above may pertain only to positive IOD phases.

5. Summary and conclusions

We have examined the variation of the Indian Ocean deep meridional overturning circulation (DMOC) in relation to IOD events using GECCO synthesis. To assess the relative importance of various dynamical processes in causing the seasonal cycle of the DMOC and in imprinting IOD influences down into the deep ocean, the DMOC is decomposed into four components (following Hirschi and Marotzke 2007): the Ekman flow plus a barotropic compensation, vertically sheared flows comprising the thermal wind, the external mode accounting for zonally varying topography, and a residual term including ageostrophic flow associated with friction and nonlinear effects. The residual term remains relatively small on seasonal to interannual time scales and thus is not discussed in detail in this study (Figs. 4c and 7f).

The Ekman component determines the overall seasonal structure of the DMOC and contributes to a

substantial part of the amplitude throughout all months. Exceptions are in the transitional seasons (March–April and September–October), when the thermal wind component has the same sign in the entire Indian Ocean Basin with amplitude comparable to that of the Ekman contribution. In fact, in the northern Indian Ocean Basin the thermal wind component offsets the Ekman contribution and determines the local DMOC structure. The external mode causes moderate seasonal variations at latitudes where the Somali Current and the corresponding gyre reverse their directions seasonally (Lee and Marotzke 1998). It shares the same sign south of 20°S with the concurrent Ekman component, suggesting its close link to the seasonally reversed wind pattern both sides of 20°S (Fig. 2) and thus also to the related Ekman drift.

The composite analysis of the three dynamical components of the DMOC reveals that each component plays a different role during different IOD phases. In May–June, the IOD-related DMOC structure is characterized by a dipole pattern separated at around 10°S , which is mainly contributed by the Ekman component, whereas from July to December the contribution of the geostrophic component increases considerably and determines the main DMOC feature. These changes in the relative contribution of the Ekman and thermal wind components of the DMOC relate closely to the surface features at different IOD phases: namely, the IOD-related SST anomalies and the associated wind anomalies.

Acknowledgments. This work is supported by the NSFC (41376024); the Strategic Priority Research Program (XDA11010301); the “Hundred Talents Program”

and External Cooperation Program of BIC (GJHZ201319) from CAS; the Science and Technology Program of Guangzhou, China (12F084060027); the National Basic Research Program of China (2013CB430301); and the Cluster of Excellence “CliSAP” from Universität Hamburg (EXC177). We are thankful to three anonymous reviewers, whose suggestions and comments have helped improve the manuscript.

REFERENCES

- Annamalai, H., and R. Murtugudde, 2004: Role of the Indian Ocean in regional climate variability. *Earth's Climate: The Ocean-Atmosphere Interaction, Geophys. Monogr.*, Vol. 147, Amer. Geophys. Union, 213–246.
- Brandt, P., L. Stramma, F. Schott, J. Fischer, M. Dengler, and D. Quadfasel, 2002: Annual Rossby waves in the Arabian Sea from TOPEX/POSEIDON altimeter and in situ data. *Deep-Sea Res. II*, **49**, 1197–1210, doi:10.1016/S0967-0645(01)00166-7.
- Bryden, H. L., and L. M. Beal, 2001: Role of the Agulhas Current in Indian Ocean circulation and associated heat and freshwater fluxes. *Deep-Sea Res. I*, **48**, 1821–1845, doi:10.1016/S0967-0637(00)00111-4.
- Chirokova, G., and P. J. Webster, 2006: Interannual variability of Indian Ocean heat transport. *J. Climate*, **19**, 1013–1031, doi:10.1175/JCLI3676.1.
- Drijfhout, S. S., and A. C. N. Garabato, 2008: The zonal dimension of the Indian Ocean meridional overturning circulation. *J. Phys. Oceanogr.*, **38**, 359–379, doi:10.1175/2007JPO3640.1.
- Du, Y., W. Cai, and Y. Wu, 2013: A new type of the Indian Ocean dipole since the mid-1970s. *J. Climate*, **26**, 959–972, doi:10.1175/JCLI-D-12-00047.1.
- Feng, M., and G. Meyers, 2003: Interannual variability in the tropical Indian Ocean: A two-year time-scale of Indian Ocean dipole. *Deep-Sea Res. II*, **50**, 2263–2284, doi:10.1016/S0967-0645(03)00056-0.
- Ferron, B., and J. Marotzke, 2003: Impact of 4D-variational assimilation of WOCE hydrography on the meridional circulation of the Indian Ocean. *Deep-Sea Res. II*, **50**, 2005–2021, doi:10.1016/S0967-0645(03)00043-2.
- Ganachaud, A., 2003: Large-scale mass transports, water mass formation, and diffusivities estimated from World Ocean Circulation Experiment (WOCE) hydrographic data. *J. Geophys. Res.*, **108**, 3213, doi:10.1029/2002JC001565.
- , and C. Wunsch, 2000: Improved estimates of global ocean circulation, heat transport and mixing from hydrographic data. *Nature*, **408**, 453–457, doi:10.1038/35044048.
- , —, J. Marotzke, and J. Toole, 2000: Meridional overturning and large-scale circulation of the Indian Ocean. *J. Geophys. Res.*, **105**, 26 117–26 134, doi:10.1029/2000JC900122.
- Garternicht, U., and F. Schott, 1997: Heat fluxes of the Indian Ocean from a global eddy-resolving model. *J. Geophys. Res.*, **102**, 21 147–21 159, doi:10.1029/97JC01585.
- Guan, Y. P., and R. X. Huang, 2008: Stommel's box model of thermohaline circulation revisited—The role of mechanical energy supporting mixing and the wind-driven gyration. *J. Phys. Oceanogr.*, **38**, 909–917, doi:10.1175/2007JPO3535.1.
- Hellerman, S., and M. Rosenstein, 1983: Normal monthly wind stress over the World Ocean with error estimates. *J. Phys. Oceanogr.*, **13**, 1093–1104, doi:10.1175/1520-0485(1983)013<1093:NMWSOT>2.0.CO;2.
- Hirschi, J., and J. Marotzke, 2007: Reconstructing the meridional overturning circulation from boundary densities and the zonal wind stress. *J. Phys. Oceanogr.*, **37**, 743–763, doi:10.1175/JPO3019.1.
- Huang, R. X., 1999: Mixing and energetics of the oceanic thermohaline circulation. *J. Phys. Oceanogr.*, **29**, 727–746, doi:10.1175/1520-0485(1999)029<0727:MAEOTO>2.0.CO;2.
- Huussen, T. N., A. C. Naveira-Garabato, H. L. Bryden, and E. L. McDonagh, 2012: Is the deep Indian Ocean MOC sustained by breaking internal waves? *J. Geophys. Res.*, **117**, C08024, doi:10.1029/2012JC008236.
- Johnson, G. C., 2011: Deep signatures of southern tropical Indian Ocean annual Rossby waves. *J. Phys. Oceanogr.*, **41**, 1958–1964, doi:10.1175/JPO-D-11-029.1.
- Kessler, W., and J. P. McCreary, 1993: The annual wind-driven Rossby wave in the subtropical equatorial Pacific. *J. Phys. Oceanogr.*, **23**, 1192–1206, doi:10.1175/1520-0485(1993)023<1192:TAWDRW>2.0.CO;2.
- Köhl, A., and D. Stammer, 2008a: Variability of the meridional overturning in the North Atlantic from the 50-year GECCO state estimation. *J. Phys. Oceanogr.*, **38**, 1913–1930, doi:10.1175/2008JPO3775.1.
- , and —, 2008b: Decadal sea level changes in the 50-year GECCO ocean synthesis. *J. Climate*, **21**, 1876–1890, doi:10.1175/2007JCLI2081.1.
- , D. Dommenges, K. Ueyoshi, and D. Stammer, 2006: The global ECCO 1952 to 2001 ocean synthesis. ECCO Rep. 40, 44 pp. [Available online at http://www.ecco-group.org/ecco/report/report_40.pdf.]
- , D. Stammer, and B. Cornuelle, 2007: Interannual to decadal changes in the ECCO global synthesis. *J. Phys. Oceanogr.*, **37**, 313–337, doi:10.1175/JPO3014.1.
- Lee, T., and J. Marotzke, 1998: Seasonal cycles of meridional overturning and heat transport of the Indian Ocean. *J. Phys. Oceanogr.*, **28**, 923–943, doi:10.1175/1520-0485(1998)028<0923:SCOMOA>2.0.CO;2.
- Liu, Y., M. Feng, J. Church, and D. Wang, 2005: Effect of salinity on estimating geostrophic transport of the Indonesian Throughflow along the IX1 XBT section. *J. Oceanogr.*, **61**, 795–801, doi:10.1007/s10872-005-0086-3.
- Loschnigg, J., G. A. Meehl, P. J. Webster, J. M. Arblaster, and G. P. Compo, 2003: The Asian monsoon, the tropospheric biennial oscillation, and the Indian Ocean zonal mode in the NCAR CSM. *J. Climate*, **16**, 1617–1642, doi:10.1175/1520-0442(2003)016<1617:TAMTTB>2.0.CO;2.
- Lumpkin, R., and K. Speer, 2007: Global ocean meridional overturning. *J. Phys. Oceanogr.*, **37**, 2550–2562, doi:10.1175/JPO3130.1.
- Macdonald, A. M., 1998: The global ocean circulation: A hydrographic estimate and regional analysis. *Prog. Oceanogr.*, **41**, 281–382, doi:10.1016/S0079-6611(98)00020-2.
- Mantyla, A. W., and J. L. Reid, 1995: On the origins of deep and bottom waters of the Indian Ocean. *J. Geophys. Res.*, **100**, 2417–2439, doi:10.1029/94JC02564.
- McDonagh, E. L., H. L. Bryden, B. A. King, and R. J. Sanders, 2008: The circulation of the Indian Ocean at 32°S. *Prog. Oceanogr.*, **79**, 20–36, doi:10.1016/j.pocean.2008.07.001.
- Meehl, G. A., and J. M. Arblaster, 2002: The tropospheric biennial oscillation and Asian–Australian monsoon rainfall. *J. Climate*, **15**, 722–744, doi:10.1175/1520-0442(2002)015<0722:TTBOAA>2.0.CO;2.
- Nycander, J., J. Nilsson, K. Doos, and G. Brostrom, 2007: Thermodynamic analysis of ocean circulation. *J. Phys. Oceanogr.*, **37**, 2038–2052, doi:10.1175/JPO3113.1.

- Palmer, M. D., A. C. Naveira Garabato, J. D. Stark, J. J.-M. Hirschi, and J. Marotzke, 2007: The influence of diapycnal mixing on quasi-steady overturning states in the Indian Ocean. *J. Phys. Oceanogr.*, **37**, 2290–2304, doi:10.1175/JPO3117.1.
- Pillai, P. A., 2008: Studies on the role of tropospheric biennial oscillation in the interannual variability of Indian summer monsoon. Ph.D dissertation, Cochin University of Science and Technology, 167 pp.
- , and K. Mohankumar, 2009: Role of TBO and ENSO scale ocean–atmosphere interaction in the Indo-Pacific region on Asian summer monsoon variability. *Theor. Appl. Climatol.*, **97**, 99–108, doi:10.1007/s00704-008-0053-1.
- Rintoul, S. R., and Coauthors, 2010: Deep circulation and meridional overturning: Recent progress and a strategy for sustained observations. *Proc. OceanObs'09: Sustained Ocean Observations and Information for Society*, Venice, Italy, ESA Publ. WPP-306, doi:10.5270/OceanObs09.pp.32.
- Robbins, P. E., and J. M. Toole, 1997: The dissolved silica budget as a constraint on the meridional overturning circulation of the Indian Ocean. *Deep-Sea Res. I*, **44**, 879–906, doi:10.1016/S0967-0637(96)00126-4.
- Saji, N. H., and T. Yamagata, 2003: Structure of SST and surface wind variability during Indian Ocean dipole mode events: COADS observations. *J. Climate*, **16**, 2735–2751, doi:10.1175/1520-0442(2003)016<2735:SOSASW>2.0.CO;2.
- , B. N. Goswami, P. N. Vinayachandran, and T. Yamagata, 1999: A dipole mode in the tropical Indian Ocean. *Nature*, **401**, 360–363.
- Schott, F. A., and J. P. McCreary, 2001: The monsoon circulation of the Indian Ocean. *Prog. Oceanogr.*, **51**, 1–123, doi:10.1016/S0079-6611(01)00083-0.
- , M. Dengler, and R. Schoenfeldt, 2002: The shallow overturning circulation of the Indian Ocean. *Prog. Oceanogr.*, **53**, 57–103, doi:10.1016/S0079-6611(02)00039-3.
- Sloyan, B. M., and S. R. Rintoul, 2001: The Southern Ocean limb of the global deep overturning circulation. *J. Phys. Oceanogr.*, **31**, 143–173, doi:10.1175/1520-0485(2001)031<0143:TSOLOT>2.0.CO;2.
- Stammer, D., and Coauthors, 2002: Global ocean circulation during 1992–1997, estimated from ocean observations and a general circulation model. *J. Geophys. Res.*, **107**, 3118, doi:10.1029/2001JC000888.
- , K. Ueyoshi, A. Köhl, W. G. Large, S. A. Josey, and C. Wunsch, 2004: Estimating air-sea fluxes of heat, freshwater, and momentum through global ocean data assimilation. *J. Geophys. Res.*, **109**, C05023, doi:10.1029/2003JC002082.
- Thompson, D. W. J., and J. M. Wallace, 2000: Annular modes in the extratropical circulation. Part I: Month-to-month variability. *J. Climate*, **13**, 1000–1016, doi:10.1175/1520-0442(2000)013<1000:AMITEC>2.0.CO;2.
- Toole, J. M., and B. A. Warren, 1993: A hydrographic section across the subtropical south Indian Ocean. *Deep-Sea Res. II*, **40**, 1973–2019, doi:10.1016/0967-0637(93)90042-2.
- Ummerhofer, C. C., F. U. Schwarzkopf, G. Meyers, E. Behrens, A. Biastoch, and C. W. Böning, 2013: Pacific Ocean contribution to the asymmetry in eastern Indian Ocean variability. *J. Climate*, **26**, 1152–1171, doi:10.1175/JCLI-D-11-00673.1.
- Wang, W., A. Köhl, and D. Stammer, 2010: Estimates of global ocean volume transports during 1960 through 2001. *Geophys. Res. Lett.*, **37**, L15601, doi:10.1029/2010GL043949.
- , —, and —, 2012: The deep meridional overturning circulation in the Indian Ocean inferred from the GECCO synthesis. *Dyn. Atmos. Oceans*, **58**, 44–61, doi:10.1016/j.dynatmoce.2012.08.001.
- Webster, P. J., A. Moore, J. Loschnigg, and M. Leban, 1999: Coupled ocean-atmosphere dynamics in the Indian Ocean during 1997–98. *Nature*, **401**, 356–360, doi:10.1038/43848.
- , C. Clark, G. Cherikova, J. Fasullo, W. Han, J. Loschnigg, and K. Sahami, 2002: The monsoon as a self-regulating coupled ocean-atmosphere system. *Meteorology at the Millennium*, R. P. Pearce, Ed., Academic Press, 198–219.
- White, W. B., 2000a: Coupled Rossby waves in the Indian Ocean on interannual timescales. *J. Phys. Oceanogr.*, **30**, 2972–2988, doi:10.1175/1520-0485(2001)031<2972:CRWITI>2.0.CO;2.
- , 2000b: Tropical coupled Rossby waves in the Pacific ocean–atmosphere system. *J. Phys. Oceanogr.*, **30**, 1245–1264, doi:10.1175/1520-0485(2000)030<1245:TCRWIT>2.0.CO;2.
- , 2001: Evidence for coupled Rossby waves in the annual cycle of the Indo-Pacific Ocean. *J. Phys. Oceanogr.*, **31**, 2944–2957, doi:10.1175/1520-0485(2001)031<2944:EFCRWI>2.0.CO;2.
- Xie, S.-P., H. Annamalai, F. A. Schott, and J. P. McCreary, 2002: Structure and mechanisms of south Indian Ocean climate variability. *J. Climate*, **15**, 864–878, doi:10.1175/1520-0442(2002)015<0864:SAMOSI>2.0.CO;2.